

Article

Composed Effects of Electron-Hole Exchange and Near-Field Interaction in Quantum-Dot-Confined Radiative Dipoles

Jaime David Díaz-Ramírez ¹, Shiang-Yu Huang ², Bo-Long Cheng ², Ping-Yuan Lo ², Shun-Jen Cheng ^{2,*}
and Hanz Yecid Ramírez-Gómez ^{1,*}

¹ Grupo de Física Teórica y Computacional & Grupo QUCIT, Escuela de Física, Universidad Pedagógica y Tecnológica de Colombia, Tunja 150003, Colombia

² Department of Electrophysics, National Yang Ming Chiao Tung University, Hsinchu 300, Taiwan

* Correspondence: sjcheng@nycu.edu.tw (S.-J.C.); hanz.ramirez@uptc.edu.co (H.Y.R.-G.)

Abstract: Conservation of polarization is an important requirement for reliable single-photon emitters, which, in turn, are essential building blocks for light-based quantum information processing. In this work, we study the exciton-spin dynamics in a double quantum dot under the combined effects of electron-hole exchange and Förster resonance energy transfer. By means of numerical solutions of the quantum master equation, we simulate the time-dependent spin polarization for two neighboring dots. According to our results, under some conditions, the depolarization caused by the electron-hole exchange may be slowed by the near field-induced interdot energy transfer, suggesting a new mechanism to extend the exciton coherence time. This opens doors to alternative schemes for improved solid-state quantum light sources.

Keywords: quantum dots; electron-hole exchange; decoherence; fine structure splitting; Förster resonance energy transfer; polarized emission; dipole-dipole interaction



Citation: Díaz-Ramírez, J.D.; Huang, S.-Y.; Cheng, B.-L.; Lo, P.-Y.; Cheng, S.-J.; Ramírez-Gómez, H.Y.

Composed Effects of Electron-Hole Exchange and Near-Field Interaction in Quantum-Dot-Confined Radiative Dipoles. *Condens. Matter* **2023**, *8*, 84. <https://doi.org/10.3390/condmat8030084>

Academic Editors: Alexey Kavokin and Helgi Sigurdsson

Received: 31 July 2023

Revised: 4 September 2023

Accepted: 11 September 2023

Published: 16 September 2023



Copyright: © 2023 by the authors. Licensee MDPI, Basel, Switzerland. This article is an open access article distributed under the terms and conditions of the Creative Commons Attribution (CC BY) license (<https://creativecommons.org/licenses/by/4.0/>).

1. Introduction

At present, semiconductor quantum dots (QDs) are of great interest for the advancement of different optoelectronic technologies, including single-photon emission and the generation of entangled photon pairs for light-based quantum information [1–4]. However, the exciton fine structure splitting (FSS), underlain by the electron-hole exchange interaction, remains a serious obstacle for industrial-scale utilization. That splitting between bright exciton states is transversal to QDs of different types and compositions since it is related to intrinsic asymmetries in shape or defect presence [5–9]. Hence, different QD growth techniques and the application of external fields have been explored to find mechanisms for the reduction of such splitting [10–13].

The loss of exciton polarization is a particularly undesirable effect of the electron-hole exchange, that mixes states with well-defined angular momentum and destroys the exciton-spin coherence, which otherwise would remain almost unaffected during the exciton lifetime [14–16].

The interaction between neighboring QDs mediated by photons, phonons and plasmons have been previously studied [17–21]. It has been found that interdot interactions may provide additional possibilities for charge and spin control, thus favoring coupled dots for applications that require high tunability. Additionally, those studies revealed that interactions between dots cannot be neglected in QD arrays in which the dots are separated by distances of a few tens of nanometers or less [22–27]. In particular, if the QDs are close enough, near-field electrodynamic interactions yield exciton population transfer [22,28,29].

In this work, we consider the combined effects of electron-hole exchange and Förster resonance energy transfer. Both are commonly described in terms of dipole-dipole interactions, becoming relevant in similar spatial ranges and energy scales. Nevertheless, the former mainly has an intradot character, while the latter is of interdot nature [23,25–27].

In what follows, the composed influence of these two polarization decoherence channels on the spin dynamics of an optically generated bright exciton in a double QD is presented in the framework of the Lindblad master equation. Such an equation is numerically solved for different relative positions between dots so that geometrical configurations in which the polarization coherence is extended compared to the single dot case, are found.

2. Hamiltonian and Theoretical Model

To include the above mentioned interactions, the total Hamiltonian of the system reads

$$\hat{H}_S = \hat{H}_{D1} + \hat{H}_{D2} + \hat{H}_{EX} + \hat{H}_{FT} \tag{1}$$

where \hat{H}_{D1} (\hat{H}_{D2}) is the confinement Hamiltonian for carriers trapped in the dot number 1 (2) and \hat{H}_{EX} (\hat{H}_{FT}) is the part corresponding to the electron-hole exchange (Förster energy transfer).

2.1. Quantum Dot Model

Within the single band effective mass approximation, the wave function $\psi_{n,m}^b(\vec{r})$ of a single carrier in the band $b = v, c$ (whether valence or conduction), confined in either of the quantum dots, is given by

$$\psi_{n,m}^b(\vec{r}) = g_n^b(\vec{r})u_m^b(\vec{r}) \tag{2}$$

where $g_n(\vec{r})$ is the wave function of the n envelope orbital and $u_m^b(\vec{r})$ is the corresponding Bloch wave function with z -projection of orbital angular momentum m .

We model the quantum dots as hard spheres with radius a [30–32], whose envelope wave function is obtained by solving the equation

$$\left[-\frac{\hbar^2}{2m_b^*} \nabla^2 + V^b(\vec{r}) \right] g_{n_b}^b(\vec{r}) = E_{n_b}^b g_{n_b}^b(\vec{r}) , \tag{3}$$

where the confinement potential is

$$V^v(\vec{r}) = V^c(\vec{r}) = \begin{cases} 0 & \text{For } r < a \\ \infty & \text{For } r \geq a \end{cases} . \tag{4}$$

The solution of Equation (3) yields the envelope wave functions

$$g_{n_b}^b(r, \theta, \phi) = \sqrt{\frac{2}{a^3}} \frac{J_l\left(\frac{\alpha_{l,n_b} r}{a}\right)}{J_{l+1}(\alpha_{l,n_b})} Y_l^m(\theta, \phi) , \tag{5}$$

where α_{l,n_b} is the n_b -th root of the spherical Bessel function of the first kind ($J_l(x)$) of order l -th, while $Y_l^m(\theta, \phi)$ are the standard spherical harmonics.

In turn, the confinement Eigenenergies are obtained according to

$$E_{n_b}^b = \frac{\hbar^2 \alpha_{l,n_b}^2}{2m_b^* a^2} . \tag{6}$$

We will restrict our study to the first envelope orbital in the valence and conduction bands ($n_v = n_c = 0$). Thus, with respect to the system ground state (no electrons in the conduction band), the energy of the neutral exciton state is

$$E_g^{QD} = E_g + \frac{\hbar^2 \alpha_{0,0}^2}{2a^2} \frac{1}{\mu^*} , \tag{7}$$

where $\frac{1}{\mu^*} = \frac{1}{m_c^*} + \frac{1}{m_v^*}$ is the electron and hole-reduced effective mass and E_g is the strained energy gap of the material.

2.2. Electron-Hole Exchange

Because of significant wave function overlapping in single QDs, electron-hole (e-h) pairs are subject to the spin-dependent exchange interaction, whose magnitude is given by the exchange integral

$$V_{n_v, m_v; n_c, m_c | n'_v, m'_v; n'_c, m'_c}^{EX} = \int \int \psi_{n_v, m_v}^{v*}(\vec{r}_1) \psi_{n_c, m_c}^{c*}(\vec{r}_2) \frac{e^2}{4\pi\epsilon_0\epsilon_b |\vec{r}_2 - \vec{r}_1|} \psi_{n'_v, m'_v}^v(\vec{r}_2) \psi_{n'_c, m'_c}^c(\vec{r}_1) d^3r_1 d^3r_2, \quad (8)$$

where e is the electron charge, and ϵ_r is the relative permittivity of the quantum dot material. \vec{r}_1 and \vec{r}_2 are the exchanging position vectors, and $|\vec{r}_2 - \vec{r}_1|$ is the distance between the electron and hole. $\psi_{n_b, m_b}^b(\vec{r})$ ($b = v, c$) is the wave function of an electron in the conduction or a hole valence band, with the form shown in Equation (2).

Because we focus on the ground electron and hole states in this study, and only consider heavy holes in the valence band (conduction band of s character and valence band of p character with no heavy hole-light hole mixing), the e-h exchange matrix elements of interest are reduced to

$$V_{0, j_z; 0, s_z | 0, j'_z; 0, s'_z}^{EX} = \int \int \psi_{0, j_z}^{v*}(\vec{r}_1) \psi_{0, s_z}^{c*}(\vec{r}_2) \frac{e^2}{4\pi\epsilon_0\epsilon_b |\vec{r}_2 - \vec{r}_1|} \psi_{0, j'_z}^v(\vec{r}_2) \psi_{0, s'_z}^c(\vec{r}_1) d^3r_1 d^3r_2, \quad (9)$$

where $j_z, j'_z = \pm\frac{3}{2}$ and $s_z, s'_z = \pm\frac{1}{2}$ are the only relevant quantum numbers for the z -projection of total angular momentum for each hole and electron.

Furthermore, since only optically active excitons (bright excitons) are of importance for the studied problem, we pay attention only to the cases in which $j_z + s_z = \pm 1$ and $j'_z + s'_z = \pm 1$. From the four remaining cases, those where $j_z + s_z = -(j'_z + s'_z)$ [$j_z + s_z = (j'_z + s'_z)$] are related to spin-flipping (conserving) processes.

Regarding exciton-spin polarization, the e-h exchange interaction involving spin flipping is the main cause of spin decoherence and the main obstacle to robust polarization-defined light emission from quantum dots. The magnitude of this interaction is then determined by $|V_{0, \frac{3}{2}; 0, -\frac{1}{2} | 0, -\frac{3}{2}; 0, \frac{1}{2}}^{EX}| = |V_{0, -\frac{3}{2}; 0, \frac{1}{2} | 0, \frac{3}{2}; 0, -\frac{1}{2}}^{EX}|$, which may be obtained from experimental measurements of the exciton fine structure splitting (FSS), available in the literature for various types of QDs [33].

2.3. Förster Resonance Energy Transfer

Bright excitons have an associated interband transition dipole whose magnitude determines the strength of radiation-matter coupling. When two of those dipoles are separated by nanometric distances and have similar excitation energies, energy may be passed from one another through the mechanism known as Förster resonance energy transfer (FRET), which is commonly approached in terms of a non-radiative dipole-dipole interaction, according to

$$V_{\vec{\mu}_{n_v, j_z^1; m_c^1, s_z^1}^1 | \vec{\mu}_{n_v, j_z^2; m_c^2, s_z^2}^2}^{FT} \approx \frac{1}{4\pi\epsilon_0\epsilon_b} \left[\frac{\left(\vec{\mu}_{n_v, j_z^1; m_c^1, s_z^1}^1 \cdot \vec{\mu}_{n_v, j_z^2; m_c^2, s_z^2}^2 \right) - 3 \left(\vec{\mu}_{n_v, j_z^1; m_c^1, s_z^1}^1 \cdot \hat{\delta}_{21} \right) \times \left(\vec{\mu}_{n_v, j_z^2; m_c^2, s_z^2}^2 \cdot \hat{\delta}_{21} \right)}{|\vec{O}_{21}|^3} \right], \quad (10)$$

where \vec{O}_{21} is the center to center interdot vector and $\hat{\delta}_{21} = \frac{\vec{O}_{21}}{|\vec{O}_{21}|}$ is its unit vector. μ_i represents the transition dipole associated to the neutral exciton in the i -th QD ($i = 1, 2$), defined as

$$\vec{\mu}_{n_v, j_z^i; m_c^i, s_z^i}^i = e \langle \psi_{n_v, j_z^i}^v | \vec{r}_i | \psi_{n_c, s_z^i}^c \rangle = e \int \psi_{n_v, j_z^i}^{v*}(\vec{r}_i) \vec{r}_i \psi_{n_c, s_z^i}^c(\vec{r}_i) d^3r_i. \quad (11)$$

In Figure 1a, the pair of interacting dipoles associated to the neighboring QDs are depicted.

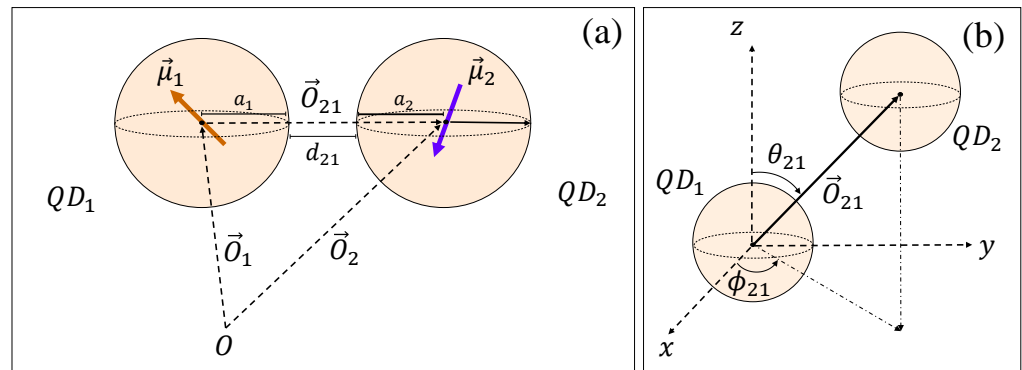


Figure 1. Schematics of the studied system. (a) Depiction of two interacting dipoles, each corresponding to one quantum dot. $|\vec{O}_{21}| = a_1 + a_2 + d_{21}$. (b) Coordinate system and definition of the angles θ_{21} and ϕ_{21} .

Inserting in Equation (11) the wave functions described in Equation (2) yields the FRET interaction with matrix elements of the form

$$V_{n_b^1, j_z^1, n_c^1, s_z^1 | n_b^2, j_z^2, n_c^2, s_z^2}^{FT} = \frac{e^2}{4\pi\epsilon_0\epsilon_b} F_{n_b^1, n_c^1} F_{n_b^2, n_c^2}^* \times \left[\frac{(\vec{D}_{j_z^1, s_z^1} \cdot \vec{D}_{j_z^2, s_z^2}^*) - 3(\vec{D}_{j_z^1, s_z^1} \cdot \hat{\delta}_{21}) \times (\vec{D}_{j_z^2, s_z^2}^* \cdot \hat{\delta}_{21})}{|\vec{O}_{21}|^3} \right], \quad (12)$$

in terms of the envelope overlap integrals

$$F_{n_b^i, n_c^i} = \langle g_{n_b^i}^v | g_{n_c^i}^c \rangle = \int g_{n_b^i}^{v*}(\vec{R}_i) g_{n_c^i}^c(\vec{R}_i) d^3 R_i, \quad (13)$$

and the microscopic dipole integrals

$$\vec{D}_{j_z^i, s_z^i} = e \langle u_{j_z^i}^v | \vec{\tau}_i | u_{s_z^i}^e \rangle = \frac{e}{\Delta V} \int_{UC} u_{j_z^i}^{v*}(\vec{\tau}_i) \vec{\tau}_i u_{s_z^i}^e(\vec{\tau}_i) d^3 \tau_i, \quad (14)$$

where the integration vector \vec{R}_i sweeps over the whole i -th QD, while $\vec{\tau}_i$ lies within the corresponding crystal unit cell of volume ΔV .

Taking into account the restrictions mentioned in the previous subsection ($n_b^i = n_c^i = 0$, $j_z^i = \pm \frac{3}{2}$ and $s_z^i = \pm \frac{1}{2}$), we have four possibilities for the matrix elements $V_{0, j_z^1; 0, s_z^1 | 0, j_z^2; 0, s_z^2}^{FT}$. This depends on the angles θ_{21} and ϕ_{21} , which define the unit vector $\hat{\delta}_{21}$. Table 1 shows those elements in terms of the coefficient

$$V_0^{FT} \equiv \frac{e^2}{4\pi\epsilon_0\epsilon_b} \frac{\hbar^2}{2m_0} \times \frac{\sqrt{E_{p1}E_{p2}}}{E_{g1}^{QD} E_{g2}^{QD}} \frac{1}{|\vec{O}_{21}|^3}, \quad (15)$$

which, in turn, depends on the Kane parameter [34], defined in the framework of the $(\mathbf{k} \cdot \mathbf{p})$ theory as

$$E_{pi} = \frac{2}{m_0} \left| \langle u_{j_z^i}^e | \vec{p} | u_{s_z^i}^v \rangle \right|^2 = \frac{2}{m_0} \left| p_{cv}(\vec{0}) \right|^2. \quad (16)$$

This parameter is available in the literature for different semiconductor materials [35].

Table 1. FRET interaction energies $V_{0,j_z^1,0,s_z^1|0,j_z^2,0,s_z^2}^{FT}$ for the z-projection angular momentum quantum numbers $j_z^1, j_z^2 = \pm\frac{3}{2}$ and $s_z^1, s_z^2 = \pm\frac{1}{2}$, depending on the angles θ_{21} and ϕ_{21} .

j_z	s_z	j_z'	s_z'	$V_{0,j_z^1,0,s_z^1 0,j_z^2,0,s_z^2}^{FT}$
$\frac{3}{2}$	$-\frac{1}{2}$	$\frac{3}{2}$	$-\frac{1}{2}$	$\frac{1}{4}(1 + 3 \cos 2\theta_{21})V_0^{DD}$
$\frac{3}{2}$	$-\frac{1}{2}$	$-\frac{3}{2}$	$\frac{1}{2}$	$\frac{3}{4}(1 - \cos 2\theta_{21})e^{-i2\phi_{21}}V_0^{DD}$
$-\frac{3}{2}$	$\frac{1}{2}$	$\frac{3}{2}$	$-\frac{1}{2}$	$\frac{3}{4}(1 - \cos 2\theta_{21})e^{i2\phi_{21}}V_0^{DD}$
$-\frac{3}{2}$	$\frac{1}{2}$	$-\frac{3}{2}$	$\frac{1}{2}$	$\frac{1}{4}(1 + 3 \cos 2\theta_{21})V_0^{DD}$

3. Time Dependence

To study the spin polarization dynamics of the DQD system, we use the operator density ρ_S and the corresponding Master Equation in the Lindblad form to obtain its time evolution [36]. Namely

$$\dot{\rho}_S(t) = \frac{1}{i\hbar}[H_S, \rho_S] + L_\Gamma(\rho_S(t)) \quad (17)$$

where the Lindblad superoperator related to spontaneous emission is defined as

$$L_\Gamma(\rho_S(t)) = -\frac{1}{2} \sum_{k=1}^4 \Gamma_k (X_k^+ X_k^- \rho_S + \rho_S X_k^+ X_k^- - 2X_k^- \rho_S X_k^+) \quad (18)$$

where $k = 0, 1, 2, 3, 4$ is an index correspondingly associated to the basis states $|0, 0\rangle, |\uparrow\downarrow, 0\rangle, |\downarrow\uparrow, 0\rangle, |0, \uparrow\downarrow\rangle$ and $|0, \downarrow\uparrow\rangle$. The operator $X_k^+ = |k\rangle\langle 0, 0|$ ($X_k^- = |0, 0\rangle\langle k|$) represents the creation (annihilation) of an exciton in the basis state $|k\rangle$. In this notation, a zero on the left (right) of the comma inside a ket means no exciton in the QD1 (QD2). In contrast, a couple of arrows at either side of the comma represent an exciton in the corresponding dot. The thin (thick) arrow indicates the z-projection of the electron (hole) total angular momentum according to

$$\begin{aligned} \uparrow &\equiv s_z = \frac{1}{2} \quad , \quad \downarrow \equiv s_z = -\frac{1}{2} \quad , \\ \uparrow &\equiv j_z = \frac{3}{2} \quad \text{and} \quad \downarrow \equiv j_z = -\frac{3}{2} \quad . \end{aligned}$$

Within the Fermi Golden Rule framework, the spontaneous emission rate for the transition from a neutral exciton state ($k \neq 0$) to the ground state $|0, 0\rangle$ depends on the corresponding transition dipole moment and the transition energy, according to

$$\Gamma_k = \frac{(E_{gk}^{QD})^3 |\vec{D}_{j_z^k, s_z^k}|^2}{3\pi\epsilon\hbar^4 c^3} \quad (19)$$

As a first approach, in this work, we consider two ideally identical quantum dots, so that the four spontaneous emission rates in Equation (18) are assumed to be the same. Although this constraint could be relaxed in the proposed model (Equation (15)), for the sake of simplicity, we assume them to be the same because in any case, the Förster interaction (the magnitude of V_0^{FT}) is relevant only close to resonance between the excitation energies [37], implying very similar QD size and composition.

It is worth noting that we use QD envelope wave functions for obtaining the magnitude of the FRET interaction, while the magnitude of the exchange interaction is taken from the literature. If we also calculate the exchange interaction terms, because their values are particularly sensitive to the lateral asymmetry, we would need to introduce some slight eccentricity into the QD shape, which would lead to wave functions that are mainly those from the spherical case, plus some perturbation. Such small perturbations would not

significantly affect the FRET results because the overlap between the electron and hole wave functions would still very close to 1 (see Equation (13)) [25].

The matrix representation of the Hamiltonian system from Equation (1), to be used in Equation (17), reads in the aforementioned basis

$$H_S = \hbar \begin{bmatrix} 0 & 0 & 0 & 0 & 0 \\ 0 & \omega_1 & \delta_{eh}^{ex} & \delta_{13} & \delta_{14} \\ 0 & \delta_{eh}^{ex} & \omega_1 & \delta_{23} & \delta_{24} \\ 0 & \delta_{31} & \delta_{32} & \omega_2 & \delta_{eh}^{ex} \\ 0 & \delta_{41} & \delta_{42} & \delta_{eh}^{ex} & \omega_2 \end{bmatrix}, \quad (20)$$

where $\delta_{eh}^{ex} \equiv |V_{0, \frac{3}{2}; 0, -\frac{1}{2}}^{EX} |0, -\frac{3}{2}; 0, \frac{1}{2}|$ stands for the magnitude of the long-range part of the e-h exchange interaction [38] and $\omega_i = \frac{E_{gi}^{QD}}{\hbar}$, with $i = 1, 2$. E_{gi}^{QD} comes from Equation (7) for the i -th QD. The FRET frequencies

$$\delta_{ij} = \frac{V_{ij}^{FT}}{\hbar}, \quad (21)$$

are obtained from the corresponding interaction energies in Table 1.

Figure 2a summarizes the considered states and the different quantities appearing in the quantum master equation, while Figure 2b depicts those quantities in the DQD system.

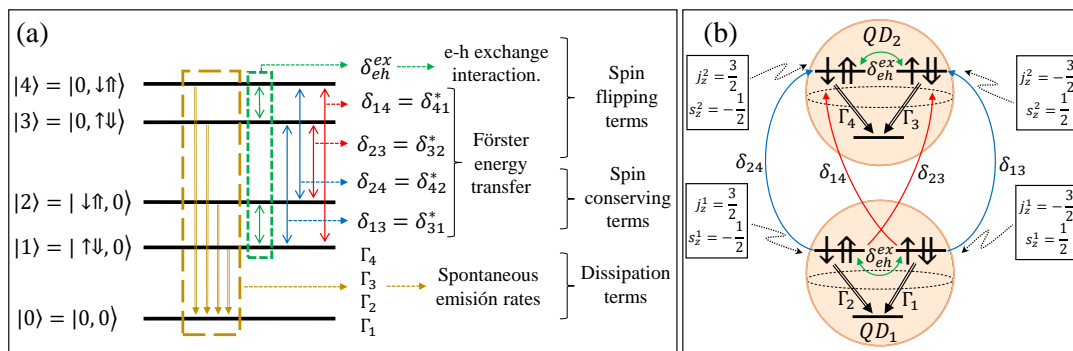


Figure 2. Schematics of the quantities describing interactions. (a) Summary of the frequencies appearing in the master equation. (b) Graphic representation of the involved states and the corresponding interactions considered in the model.

4. Results and Discussion

For the numerical simulations, we consider two identical CdSe QDs. The corresponding parameters are summarized in Table 2, which, in turn, is based on references [35,39].

Table 2. Parameters used in the numerical simulations for the pair of identical CdSe QDs.

Relevant Parameters for CdSe QDs	
QD radius ($a_1 = a_2 = a$)	3 nm
Bulk energy gap E_g (300K)	1.751 eV
QD energy gap, $E_{g1}^{QD} = E_{g2}^{QD}$	2.165 eV
Kane energy parameter E_p	17.5 eV
Electron effective mass m_e^*	0.11 m_0
Hole effective mass m_h^*	0.45 m_0
Relative permittivity ϵ_b	10
Electron-hole exchange δ_{eh}^{ex}	1 ns ⁻¹
Spontaneous emission rate Γ_k ($k = 1, 2, 3, 4$)	0.054 ns ⁻¹

The quantum master Equation (17) is numerically solved by means of the open-source software QuTiP [40]. From the obtained solutions in the chosen basis, we extract the diagonal matrix elements of the density operator in order to analyze the time evolution of the exciton-spin polarization and to compare for different geometrical configurations the lifetime of exciton configurations able to emit either σ^+ or σ^- circularly polarized photons.

Regarding initial conditions, we will suppose that at time $t = 0$ by means of σ^- polarized light from a pulsed low-power laser, the state $|\uparrow\downarrow, 0\rangle$ is optically excited in the QD1. In such a case, if the e-h exchange and Förster transfer would be negligible, the DQD would remain in that state until it would spontaneously emit a σ^- polarized photon. Thus, as long as the exciting light does not change, the photons generated in the DQD would have well-defined polarization. Furthermore, in that case, the QD2 would not be involved in the process.

Once the e-h exchange is taken into account, Rabi oscillations between the opposite polarization states within QD1 are expected. This can be observed in Figure 3a, where the Förster resonance energy transfer is neglected (i.e. a very large interdot distance is considered). In that situation, the polarization of the exciting light is lost before a couple of nanoseconds, and the emitted photons will mostly be of uncertain polarization.

If the interaction to neglect would be the e-h exchange (i.e. the involved quantum dots have an exceptionally high rotational symmetry) and the spin-flipping FRET terms would be zero ($\theta_{21} = 0$), then the Rabi oscillations would be held between the two states sharing the same exciton-spin in the DQD. Such a case is shown in Figure 3b, where δ_{eh}^{ex} and δ_{14} have been taken to be zero. There, the excitation transfer between QD1 (dashed line) and QD2 (dotted line) can be clearly observed. After the exciton radiative lifetime, spontaneous emission of a photon with σ^- polarization can be expected, although there is no certainty on what QD it will come from. However, it is remarkable that the exciton-spin is preserved despite the interdot energy transfer. Figure 3c presents the addition of the diagonal density matrix elements corresponding to equal polarization: $\rho_{11} + \rho_{33}$ on the one hand (blue solid line) and $\rho_{22} + \rho_{44}$ on the other (red solid line).

In both of the addressed cases so far, and in the ones to be discussed in what follows, the increase in the ground state population $\rho_{0,0}$ (black dash-dot line) can be observed. This is due to the spontaneous emission from exciton states that act as a dissipation channel in the DQD system.

While the dependence on ϕ_{21} is irrelevant for the general evolution of the system in the absence of spin-flipping terms (see Table 1), in all cases, the dependence on θ_{21} modulates significantly the magnitude of the spin-conserving interdot terms, as well as the difference between spin-conserving and spin-flipping FRET terms. Once non-negligible FRET and e-h exchange terms are simultaneously considered, a complex interplay of the two interactions on the time evolution of the diagonal density matrix elements leads to different scenarios, some of which are more or less convenient toward the purpose of extending exciton-spin coherence times.

In Figure 4, three different case studies are presented. Remarkably, in the third one whose angular parameters are $\theta_{21} = 0.2\pi$ and $\phi_{21} = \pi/2$, the exciton-spin coherence is clearly favored since the blue polarization is retained for a time, which is evidently longer than that in which no FRET terms are included (see Figure 3a).

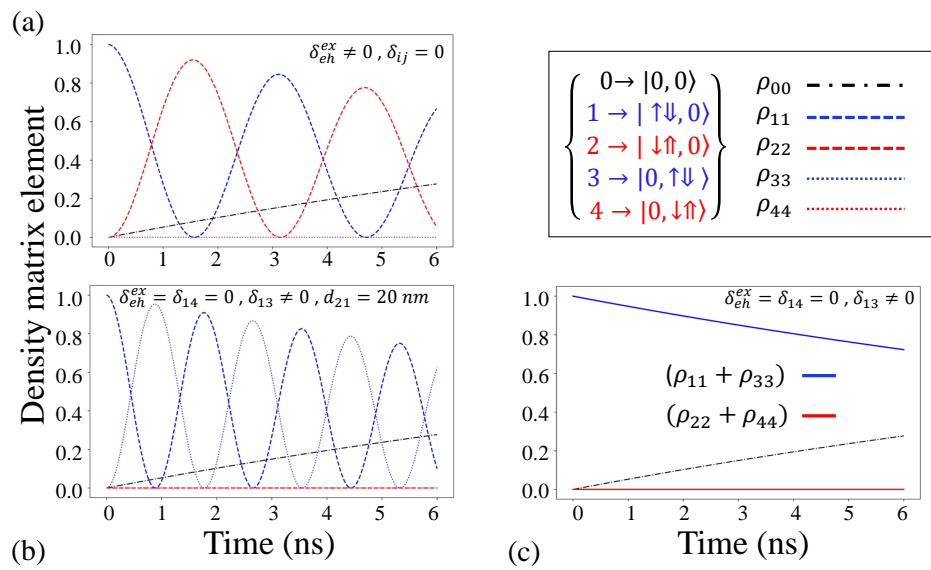


Figure 3. Density matrix elements ρ_{00} (black dash-dot line), ρ_{11} (blue dashed line), ρ_{22} (red dashed line), ρ_{33} (blue dotted line) and ρ_{44} (red dotted line) as functions of time (ns). A spontaneous emission rate $\Gamma_k = 0.054 \text{ ns}^{-1}$ and an interdot distance $d_{21} = 20 \text{ nm}$ are considered. (a) The FRET interaction is neglected ($\delta_{ij} = 0$). An e-h exchange energy of $\delta_{eh}^{ex} = 1 \text{ ns}^{-1}$ is taken. The inset shows the correspondence between colors and polarizations. (b) The e-h exchange is neglected ($\delta_{eh}^{ex} = 0$). Angles $\theta_{21} = 0$ and $\phi_{21} = 0$ are considered. (c) Addition of the density matrix elements corresponding to the same polarization. The same parameters as in (b) are used.

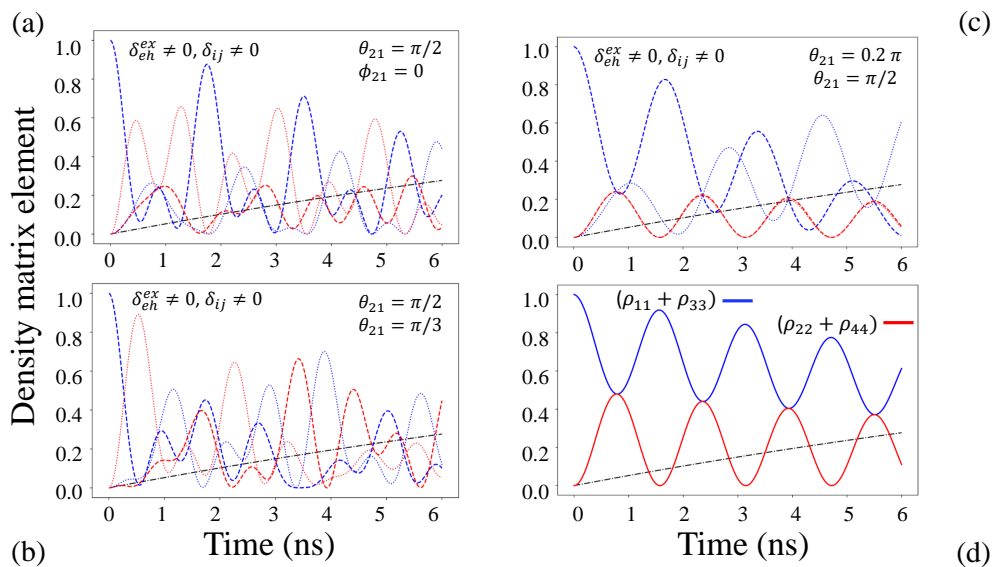


Figure 4. Density matrix elements ρ_{00} (black dash-dot line), ρ_{11} (blue dashed line), ρ_{22} (red dashed line), ρ_{33} (blue dotted line) and ρ_{44} (red dotted line) as functions of time (ns) for three different angle parameters. A spontaneous emission rate $\Gamma_k = 0.054 \text{ ns}^{-1}$, an interdot distance $d_{21} = 20 \text{ nm}$ and an e-h exchange energy $\delta_{eh}^{ex} = 1 \text{ ns}^{-1}$ are considered. (a) $\theta_{21} = \pi/2, \phi_{21} = 0$. (b) $\theta_{21} = \pi/2, \phi_{21} = \pi/3$. (c) $\theta_{21} = 0.2\pi, \phi_{21} = \pi/2$. (d) Sum of the diagonal density matrix elements that share exciton-spin polarization for the case shown in (c).

According to Figure 4d, for that DQD system, the probability of emitting a σ^- polarized photon after radiative recombination of the e-h pair is substantially bigger than the probability of emitting a σ^+ one. This suggests a new scheme for protecting exciton-spin coherence from the decoherence introduced by the e-h exchange in strongly confined double dot structures.

The case shown in Figure 4c,d is intentionally chosen to highlight the possibility of extending the exciton spin polarization. Albeit it is a specific situation, it is not at all isolated or accidental. As learned from Table 1, small values of θ_{21} tend to cancel out the interdot spin-flipping matrix elements of the Hamiltonian (despite the value of ϕ_{21}), while they maximize the spin-conserving interdot transition (see Figure 4b). Intuition tells us that preservation of the polarization is helped by the spin-conserving interdot transfer because it weakens the action of the intradot processes, including the exchange interaction that flips the spin. Thus, configurations with vertical interdot coupling (along the direction of the excited dipole) would enhance the polarization lifetime as compared with configurations where the interdot coupling is lateral (perpendicular to the direction of the excited dipole).

Regarding the experimental feasibility of taking advantage of this composed effect, it is important to mention that the fabrication of QD ensembles with nanometric interdot distance has been achieved in epitaxial and colloidal dots [41–44]. As for the angle between dots with respect to the direction of the excited dipole, it is indeed more troublesome. In colloidal QD ensembles, it should be possible to find any particular dot orientations between neighboring pairs because in those ensembles, the nanocrystals are expected to be randomly oriented. However, this randomness poses a challenge if a particular configuration is pursued. Recent advances in the obtention of nanocrystals with controlled position and shape suggest that the ability to prepare quantum dot arrays with very specific features is effectively progressing, making this proposed scheme eventually realizable [45,46].

5. Conclusions

In this work, we have presented a theoretical model to study the combined effects of the e-h exchange and the Förster resonance energy transfer in a double quantum dot. After solving the corresponding master equation for different geometrical configurations numerically, we conclude that under some conditions, it is possible to find quantum dot pairs in which the interplay between the considered interactions results in prolonged exciton-spin polarization. This opens doors to enhanced control of the polarization of emitted photons from semiconductor nanostructures, which is potentially useful for optoelectronic devices and light-based quantum information processing.

Author Contributions: Conceptualization, P.-Y.L. and S.-J.C.; Analytical calculations, S.-Y.H. and B.-L.C.; Simulations J.D.D.-R.; Manuscript outline, S.-J.C. and H.Y.R.-G.; Original draft preparation, J.D.D.-R.; Review and editing, H.Y.R.-G.; General supervision, S.-J.C. and H.Y.R.-G. All authors have read and agreed to the published version of the manuscript.

Funding: This research was funded by Sistema General de Regalías de Colombia through grant number BPIN2021000100191.

Data Availability Statement: Not applicable.

Acknowledgments: H.Y.R.-G. acknowledges support from the the Research Division of UPTC.

Conflicts of Interest: The authors declare no conflict of interest.

References

1. O'Brien, J.L.; Furusawa, A.; Vučković, J. Photonic quantum technologies. *Nat. Photonics* **2009**, *3*, 687–695. [[CrossRef](#)]
2. Chen, Y.; Zhang, J.; Zopf, M.; Jung, K.; Zhang, Y.; Keil, R.; Ding, F.; Schmidt, O.G. Wavelength-tunable entangled photons from silicon-integrated III–V quantum dots. *Nat. Commun.* **2016**, *7*, 10387. [[CrossRef](#)] [[PubMed](#)]
3. Huber, D.; Reindl, M.; Covre da Silva, S.F.; Schimpf, C.; Martín-Sánchez, J.; Huang, H.; Piredda, G.; Edlinger, J.; Rastelli, A.; Trotta, R. Strain-Tunable GaAs Quantum Dot: A Nearly Dephasing-Free Source of Entangled Photon Pairs on Demand. *Phys. Rev. Lett.* **2018**, *121*, 033902. [[CrossRef](#)]
4. Ramírez, H.Y.; Chou, Y.L.; Cheng, S.J. Effects of electrostatic environment on the electrically triggered production of entangled photon pairs from droplet epitaxial quantum dots. *Sci. Rep.* **2019**, *9*, 1547. [[CrossRef](#)]
5. Htoon, H.; Furis, M.; Crooker, S.A.; Jeong, S.; Klimov, V.I. Linearly polarized ‘fine structure’ of the bright exciton state in individual CdSe nanocrystal quantum dots. *Phys. Rev. B* **2008**, *77*, 035328. [[CrossRef](#)]
6. Htoon, H.; Crooker, S.A.; Furis, M.; Jeong, S.; Efros, A.L.; Klimov, V.I. Anomalous Circular Polarization of Photoluminescence Spectra of Individual CdSe Nanocrystals in an Applied Magnetic Field. *Phys. Rev. Lett.* **2009**, *102*, 017402. [[CrossRef](#)]

7. Gong, M.; Zhang, W.; Guo, G.C.; He, L. Exciton Polarization, Fine-Structure Splitting, and the Asymmetry of Quantum Dots under Uniaxial Stress. *Phys. Rev. Lett.* **2011**, *106*, 227401. [[CrossRef](#)] [[PubMed](#)]
8. Yin, C.; Chen, L.; Song, N.; Lv, Y.; Hu, F.; Sun, C.; Yu, W.W.; Zhang, C.; Wang, X.; Zhang, Y.; et al. Bright-Exciton Fine-Structure Splittings in Single Perovskite Nanocrystals. *Phys. Rev. Lett.* **2017**, *119*, 026401. [[CrossRef](#)] [[PubMed](#)]
9. Prin, E.; Xia, C.; Won, Y.H.; Jang, E.; Goupalov, S.V.; Tamarat, P.; Lounis, B. Revealing the Band-Edge Exciton Fine Structure of Single InP Nanocrystals. *Nano Lett.* **2023**, *23*, 6067–6072. [[CrossRef](#)]
10. Kuroda, T.; Mano, T.; Ha, N.; Nakajima, H.; Kumano, H.; Urbaszek, B.; Jo, M.; Abbarchi, M.; Sakuma, Y.; Sakoda, K.; et al. Symmetric quantum dots as efficient sources of highly entangled photons: Violation of Bell's inequality without spectral and temporal filtering. *Phys. Rev. B* **2013**, *88*, 041306. [[CrossRef](#)]
11. Gurioli, M.; Wang, Z.; Rastelli, A.; Kuroda, T.; Sanguinetti, S. Droplet epitaxy of semiconductor nanostructures for quantum photonic devices. *Nat. Mater.* **2019**, *18*, 799–810. [[CrossRef](#)]
12. Juska, G.; Dimastrodonato, V.; Mereni, L.O.; Gocalinska, A.; Pelucchi, E. Towards quantum-dot arrays of entangled photon emitters. *Nat. Photonics* **2013**, *7*, 527–531. [[CrossRef](#)]
13. Thoma, A.; Schnauber, P.; Böhm, J.; Gschrey, M.; Schulze, J.H.; Strittmatter, A.; Rodt, S.; Heindel, T.; Reitzenstein, S. Two-photon interference from remote deterministic quantum dot microlenses. *Appl. Phys. Lett.* **2017**, *110*, 011104. [[CrossRef](#)]
14. Ramirez, H.Y.; Cheng, S.J.; Chang, C.P. Theory of electron–hole exchange interaction in double quantum dots. *Phys. Status Solidi B* **2009**, *246*, 837–841. [[CrossRef](#)]
15. Ramirez, H.Y.; Lin, C.H.; You, W.T.; Huang, S.Y.; Chang, W.H.; Lin, S.D.; Cheng, S.J. Electron–hole symmetry breakings in optical fine structures of single self-assembled quantum dots. *Phys. E Low-Dimens. Syst. Nanostruct.* **2010**, *42*, 1155–1158. [[CrossRef](#)]
16. Cheng, S.J.; Liao, Y.H.; Lin, P.Y. Mechanically encoded single-photon sources: Stress-controlled excitonic fine structures of droplet epitaxial quantum dots. *Phys. Rev. B* **2015**, *91*, 115310. [[CrossRef](#)]
17. Ramirez, H.Y.; Camacho, A.S.; Lew Yan Voon, L.C. DC electric field effects on the electron dynamics in double rectangular quantum dots. *Braz. J. Phys.* **2006**, *36*, 869. [[CrossRef](#)]
18. Evans, R.E.; Bhaskar, M.K.; Sukachev, D.D.; Nguyen, C.T.; Sipahigil, A.; Burek, M.J.; Machielse, B.; Zhang, G.H.; Zibrov, A.S.; Bielejec, E.; et al. Photon-mediated interactions between quantum emitters in a diamond nanocavity. *Science* **2018**, *362*, 662–665. [[CrossRef](#)]
19. Reindl, M.; Jöns, K.D.; Huber, D.; Schimpf, C.; Huo, Y.; Zwiller, V.; Rastelli, A.; Trotta, R. Phonon-Assisted Two-Photon Interference from Remote Quantum Emitters. *Nano Lett.* **2017**, *17*, 4090–4095. [[CrossRef](#)]
20. Ramirez, H.Y.; Camacho, A.S.; Voon, L.C.L.Y. Influence of shape and electric field on electron relaxation and coherent response in quantum-dot molecules. *J. Phys. Condens. Matter* **2007**, *19*, 346216. [[CrossRef](#)]
21. Bermúdez-Ureña, E.; Gonzalez-Ballester, C.; Geiselmann, M.; Marty, R.; Radko, I.P.; Holmgaard, T.; Alaverdyan, Y.; Moreno, E.; García-Vidal, F.J.; Bozhevolnyi, S.I.; et al. Coupling of individual quantum emitters to channel plasmons. *Nat. Commun.* **2015**, *6*, 7883. [[CrossRef](#)]
22. Kim, H.; Kim, I.; Kyhm, K.; Taylor, R.A.; Kim, J.S.; Song, J.D.; Je, K.C.; Dang, L.S. Exciton Dipole–Dipole Interaction in a Single Coupled-Quantum-Dot Structure via Polarized Excitation. *Nano Lett.* **2016**, *16*, 7755–7760. [[CrossRef](#)]
23. Rolon, J.E.; Ulloa, S.E. Förster energy-transfer signatures in optically driven quantum dot molecules. *Phys. Rev. B* **2009**, *79*, 245309. [[CrossRef](#)]
24. Rolon, J.E.; Ulloa, S.E. Coherent control of indirect excitonic qubits in optically driven quantum dot molecules. *Phys. Rev. B* **2010**, *82*, 115307. [[CrossRef](#)]
25. Ramirez, H.Y.; Lin, C.H.; Chao, C.C.; Hsu, Y.; You, W.T.; Huang, S.Y.; Chen, Y.T.; Tseng, H.C.; Chang, W.H.; Lin, S.D.; et al. Optical fine structures of highly quantized InGaAs/GaAs self-assembled quantum dots. *Phys. Rev. B* **2010**, *81*, 245324. [[CrossRef](#)]
26. Kim, D.; Okahara, S.; Nakayama, M.; Shim, Y. Experimental verification of Förster energy transfer between semiconductor quantum dots. *Phys. Rev. B* **2008**, *78*, 153301. [[CrossRef](#)]
27. Unold, T.; Mueller, K.; Lienau, C.; Elsaesser, T.; Wieck, A.D. Optical Control of Excitons in a Pair of Quantum Dots Coupled by the Dipole-Dipole Interaction. *Phys. Rev. Lett.* **2005**, *94*, 137404. [[CrossRef](#)]
28. Govorov, A.O. Spin and energy transfer in nanocrystals without tunneling. *Phys. Rev. B* **2003**, *68*, 075315. [[CrossRef](#)]
29. Govorov, A.O. Spin-Förster transfer in optically excited quantum dots. *Phys. Rev. B* **2005**, *71*, 155323. [[CrossRef](#)]
30. Kuno, M. Introductory nanoscience: Physical and chemical concepts. *MRS Bull.* **2012**, *37*, 169–170. [[CrossRef](#)]
31. Zapata-Herrera, M.; Flórez, J.; Camacho, A.S.; Ramírez, H.Y. Quantum Confinement Effects on the Near Field Enhancement in Metallic Nanoparticles. *Plasmonics* **2018**, *13*, 1–7. [[CrossRef](#)]
32. Zapata-Herrera, M.; Camacho, A.S.; Ramírez, H.Y. Influence of the confinement potential on the size-dependent optical response of metallic nanometric particles. *Comput. Phys. Commun.* **2018**, *227*, 1–7. [[CrossRef](#)]
33. Huber, D.; Reindl, M.; Aberl, J.; Rastelli, A.; Trotta, R. Semiconductor quantum dots as an ideal source of polarization-entangled photon pairs on-demand: A review. *J. Opt.* **2018**, *20*, 073002. [[CrossRef](#)]
34. Chuang, S.L. *Physics of Optoelectronic Devices*; Wiley: New York, NY, USA, 1995; pp. 124–195.
35. Gywat, O.; Krenner, H.J.; Berezovsky, J. *Spins in Optically Active Quantum Dots: Concepts and Methods*; John Wiley & Sons: Hoboken, NJ, USA, 2009.
36. Carmichael, H. *Statistical Methods in Quantum Optics 1: Master Equations and Fokker-Planck Equations*; Springer Science & Business Media: Berlin, Germany, 1999; Volume 1.

37. Al-Ahmadi, A.N.; Ulloa, S.E. Coherent state monitoring in quantum dots. *Phys. Rev. B* **2004**, *70*, 201302. [[CrossRef](#)]
38. Woggon, U.; Gindele, F.; Wind, O.; Klingshirn, C. Exchange interaction and phonon confinement in CdSe quantum dots. *Phys. Rev. B* **1996**, *54*, 1506–1509. [[CrossRef](#)] [[PubMed](#)]
39. Shiang-Yu Huang, S.J.C. Theoretical Studies of Energy Transfer between Coupled Semiconductor Nanocrystals. Master's Thesis, National Chiao Tung University, HsinChu, Taiwan, China, 2015.
40. Johansson, J.; Nation, P.; Nori, F. QuTiP 2: A Python framework for the dynamics of open quantum systems. *Comput. Phys. Commun.* **2013**, *184*, 1234–1240. [[CrossRef](#)]
41. Reiss, P.; Bleuse, J.; Pron, A. Highly Luminescent CdSe/ZnSe Core/Shell Nanocrystals of Low Size Dispersion. *Nano Lett.* **2002**, *2*, 781–784. [[CrossRef](#)]
42. Heyn, C.; Stemmann, A.; Schramm, A.; Welsch, H.; Hansen, W.; Nemcsics, A. Regimes of GaAs quantum dot self-assembly by droplet epitaxy. *Phys. Rev. B* **2007**, *76*, 075317. [[CrossRef](#)]
43. Jo, M.; Mano, T.; Sakuma, Y.; Sakoda, K. Extremely high-density GaAs quantum dots grown by droplet epitaxy. *Appl. Phys. Lett.* **2012**, *100*, 212113. [[CrossRef](#)]
44. Won, Y.H.; Cho, O.; Kim, T.; Chung, D.Y.; Kim, T.; Chung, H.; Jang, H.; Lee, J.; Kim, D.; Jang, E. Highly efficient and stable InP/ZnSe/ZnS quantum dot light-emitting diodes. *Nature* **2019**, *575*, 634–638. [[CrossRef](#)]
45. Du, J.S.; Shin, D.; Stanev, T.K.; Musumeci, C.; Xie, Z.; Huang, Z.; Lai, M.; Sun, L.; Zhou, W.; Stern, N.P.; et al. Halide perovskite nanocrystal arrays: Multiplexed synthesis and size-dependent emission. *Sci. Adv.* **2020**, *6*, eabc4959. [[CrossRef](#)] [[PubMed](#)]
46. Jastrzebska-Perfect, P.; Zhu, W.; Saravanapavanantham, M.; Li, Z.; Spector, S.O.; Brenes, R.; Satterthwaite, P.F.; Ram, R.J.; Niroui, F. On-site growth of perovskite nanocrystal arrays for integrated nanodevices. *Nat. Commun.* **2023**, *14*, 3883. [[CrossRef](#)] [[PubMed](#)]

Disclaimer/Publisher's Note: The statements, opinions and data contained in all publications are solely those of the individual author(s) and contributor(s) and not of MDPI and/or the editor(s). MDPI and/or the editor(s) disclaim responsibility for any injury to people or property resulting from any ideas, methods, instructions or products referred to in the content.